



Cobalt- and nitrogen-codoped porous carbon catalyst made from core–shell type hybrid metal–organic framework (ZIF-L@ZIF-67) and its efficient oxygen reduction reaction (ORR) activity

Heejun Park, Sojin Oh, Sujeong Lee, Sora Choi, Moonhyun Oh*

Department of Chemistry, Yonsei University, 50 Yonsei-ro, Seodaemun-gu, Seoul, 120-749, South Korea



ARTICLE INFO

Keywords:
Porous carbon catalyst
Oxygen reduction reaction (ORR)
Four-electron transfer pathway
Hybrid metal–organic framework
Heteroatom-doping

ABSTRACT

The development of carbon-based oxygen reduction reaction (ORR) catalysts to substitute the expensive and unstable platinum-based ORR catalysts is of great importance for their optimal utilization in energy conversion and storage. Herein, we report the production of highly active carbon-based ORR catalyst from well-designed core–shell type hybrid metal–organic framework (MOF). Cobalt- and nitrogen-codoped porous carbon leaves (Co_xN-PCLs) are prepared via a simple one-step pyrolysis of well-designed leaf-shaped core–shell type hybrid MOFs (ZIF-L@ZIF-67, ZIF (zeolitic imidazolate framework) is a subclass of MOF), which contain two different metal ions (Zn²⁺ in core and Co²⁺ in shell) and sufficient nitrogen source with a thin flat morphology. The structural and compositional features of resulting Co_xN-PCLs are characterized using scanning electron microscopy, transmission electron microscopy, energy-dispersive X-ray spectroscopy, X-ray photoelectron spectroscopy, Raman spectroscopy, and N₂ sorption isotherms, and the analyses reveal that they possess the ideal structural and compositional features for ORR, such as numerous carbon nanotubes (CNTs), substantial Co- and N-doping, large surface area, and high pore volume while maintaining the advantageous thin leaf-shape. Owing to such unique structural and compositional features, Co_xN-PCLs display much better ORR activity than their counterparts prepared from the parent materials (ZIF-L or ZIF-67). In addition, Co_xN-PCL even shows a better electrochemical stability and a better methanol tolerance compared to commercial Pt/C material.

1. Introduction

Electrocatalytic oxygen reduction reaction (ORR) is of great importance in energy conversion and storage—e.g., in fuel cells and metal–air batteries [1–7]. Even though platinum-based catalysts are broadly employed in these days, their drawbacks, such as high cost, poor durability, and poor methanol tolerance, necessitate the development of optimal materials for ORR catalysis. Currently, many efforts are underway for the development of carbon-based ORR catalysts, which display an ORR catalytic activity comparable to that of Pt-based catalyst [8–10]. For example, Tang and co-workers developed several graphene- or graphene oxide-based materials for high performance ORR activity [11–14]. Wang and co-workers reported highly active carbon-based ORR catalysts through heteroatom-doping or creating defects [15,16]. During the development of carbon-based ORR catalysts, heteroatom-doping, with atoms such as nitrogen, phosphorous, and cobalt, can enhance the ORR activity by providing the optimal ORR active sites [17–22]. In addition, the presence of a substantial quantity

of graphitic carbon in a carbon-based ORR catalyst can also improve its ORR activity by improving the conductivity of the catalyst and thus providing fast electron transfer [23–26]. Lastly, high porosity and large surface area are important structural features of an ideal carbon-based ORR catalyst as they enable fast mass transport and easy accessibility to the ORR active sites [27–29].

Among the numerous methods, the preparation of carbon-based ORR catalysts from metal–organic framework (MOF) materials [30–34] is considered an excellent strategy because versatile compositions and structural diversities of MOFs make it possible to generate an ORR catalyst with ideal structural and compositional features. In particular, zeolitic imidazolate framework (ZIF) materials are one of the most promising precursor materials because they contain sufficient nitrogen atoms within a highly porous structure [35,36]. Indeed, several carbon-based ORR catalysts were prepared from various kinds of ZIF materials [23,24,37–39]. Herein, we developed the carbon-based ORR catalysts, cobalt- and nitrogen-codoped porous carbon leaves (denoted as Co_xN-PCLs), from the pyrolysis of well-designed core–shell type hybrid MOF

* Corresponding author.

E-mail address: moh@yonsei.ac.kr (M. Oh).

(ZIF-L@ZIF-67) containing two different metal ions (Zn^{2+} and Co^{2+}) and sufficient nitrogen source with a thin flat morphology. The resulting Co_3N -PCLs showed an excellent ORR activity with outstanding stability and methanol tolerance owing to their unique structural and compositional features.

2. Experimental section

2.1. Synthesis of ZIF-L

A precursor solution for ZIF-L was prepared by mixing $Zn(NO_3)_2 \cdot 6H_2O$ (0.59 g, 2 mmol) and HMeIm (1.30 g, 16 mmol) in 80 mL of deionized water [40]. The mixture was stirred at room temperature for 4 h. The resulting products were isolated via centrifugation (at 10,000 rpm for 10 min), washed with deionized water several times via centrifugation-redispersion, and thereafter dried in an oven at 70 °C overnight.

2.2. Synthesis of ZIF-67

A precursor solution for ZIF-67 was prepared by mixing $Co(NO_3)_2 \cdot 6H_2O$ (0.44 g, 1.5 mmol) and HMeIm (0.62 g, 7.5 mmol) in 60 mL of methanol and maintained at room temperature for 12 h. The resulting products were isolated via centrifugation (at 10,000 rpm for 10 min), washed with methanol several times via centrifugation-redispersion, and thereafter dried in an oven at 70 °C overnight.

2.3. Synthesis of core-shell ZIF-L@ZIF-67[1–4]

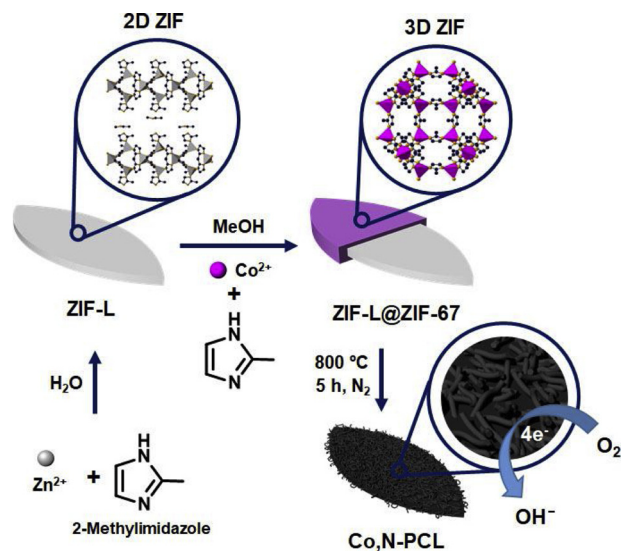
ZIF-L template (0.4 g) was mixed with $Co(NO_3)_2 \cdot 6H_2O$ (0.4, 1.6, 3.2, or 5.6 mmol were used for ZIF-L@ZIF-67[1–4], respectively) in 12 mL of methanol and thereafter, HMeIm (3.2, 12.8, 25.6, or 44.8 mmol, respectively) in 12 mL of methanol was injected. The resulting mixture was maintained at room temperature for 24 h [41,42]. The resulting products were isolated via centrifugation (at 10,000 rpm for 10 min), washed with methanol several times via centrifugation-redispersion, and thereafter dried in an oven at 70 °C overnight.

2.4. Preparation of Co_3N -PCL[1–4], C-ZIF-L, and C-ZIF-67

As-synthesized core-shell ZIF-L@ZIF-67[1–4], ZIF-L, and ZIF-67 were pyrolyzed under nitrogen at 800 °C for 5 h at a heating rate of 2 °C min⁻¹.

2.5. Electrochemical measurement

For the evaluation of ORR, all electrocatalytic measurements were performed in a three-electrode cell using a rotating disk electrode (RDE, PINE Co., Ltd.) with an electrochemical workstation Autolab potentiostat (PGSTAT128 N). An Ag/AgCl (3.0 M KCl) electrode was used as the reference electrode and a Pt foil was used as the counter electrode. The RDE with a glassy carbon (GC) disk electrode (diameter: 5 mm, area: 0.196 cm²) was used as the substrate for the working electrode. All the potentials were converted to values with respect to the reversible hydrogen electrode (RHE), $E_{RHE} = E_{Ag/AgCl} + 0.059 \times pH + 0.210$. Prior to use, the GC electrode in RDE was polished using alumina abrasive on a felt polishing pad, and was washed with ethanol and deionized water via sonication. The catalyst ink was prepared by dispersing 4 mg of catalyst in 1 mL of solution containing 0.98 mL of ethanol and 20 μ L of Nafion solution (5 wt%) followed by sonication for 1 h. Subsequently, 10 μ L of ink was dropped on the GC electrode. The geometric loading of all the catalysts including Pt/C (20 wt% platinum, Aldrich) was 0.2 mg cm⁻². Before the tests, N_2 or O_2 gas was flown for 30 min to saturate the electrolyte. The cyclic voltammetry (CV) measurement was performed in N_2 -/ O_2 -saturated 0.1 M KOH electrolyte at a scan rate of 10 mV s⁻¹. The RDE test for the ORR was performed in O_2 -saturated



Scheme 1. Schematic representation for the formation of leaf-shape ZIF-L and leaf-shape core-shell type ZIF-L@ZIF-67 and its transformation to thin Co_3N -PCL.

0.1 M KOH at different rotation rates (400–2500 rpm) at the scan rate of 10 mV s⁻¹. The electron-transfer number (n) was calculated from the Koutecky-Levich equation. For the methanol crossover test, the chronoamperometric response at 0.6 V was measured using RDE tests in O_2 -saturated 0.1 M KOH at the rotating rate of 1600 rpm, followed by the injection of 3 M methanol into 0.1 M KOH. For the electrochemical stability test, the chronoamperometric response at 0.6 V was measured using RDE tests in O_2 -saturated 0.1 M KOH at the rotating rate of 1600 rpm for 10,000 s.

3. Results and discussion

3.1. Core-shell type hybrid of ZIF-L@ZIF-67[1–4]

The synthesis of Co_3N -PCL is illustrated in **Scheme 1**. First, micro-sized leaf-shaped ZIF-L particles with a chemical composition of $[Zn(MeIm)_2(HMeIm)_{1/2}(H_2O)_{3/2}]_n$ were prepared from the room-temperature reaction between $Zn(NO_3)_2 \cdot 6H_2O$ and 2-methylimidazole (HMeIm) using a reported method (Fig. S1a,b) [40]. The formation of ZIF-L was verified from the powder X-ray diffraction (PXRD) pattern of the resulting leaf-shaped particles (Fig. S2b), which was consistent with the simulated pattern of ZIF-L (Fig. S2a). Subsequently, a series of core-shell type leaves of ZIF-L@ZIF-67 (Fig. 1 and Fig. S3–S5) was prepared from the room-temperature reaction between Co^{2+} and HMeIm in the presence of ZIF-L particles through the growth of ZIF-67 on the surface of ZIF-L template, where the amount of ZIF-67 shell portion was regulated by varying the amount of Co^{2+} and HMeIm used during the reaction while using the same amount of ZIF-L template (however, the reaction with too much Co^{2+} and HMeIm resulted in the formation of pure ZIF-67 dodecahedrons in addition to the core-shell type leaves of ZIF-L@ZIF-67, see Fig. S6). As expected, the ZIF-67-to-ZIF-L ratio within the series of core-shell particles increased with the increase in the amounts of Co^{2+} and HMeIm used during the reactions. The Co-to-Zn ratios (Co/Zn) measured from energy-dispersive X-ray spectroscopy (EDX) (Fig. S7) were 0.16, 0.57, 0.74, and 1.29. Thus, the ZIF-67-to-ZIF-L ratios for the four ZIF-L@ZIF-67 samples (denoted as ZIF-L@ZIF-67[1–4]) were approximately 0.16:1, 0.57:1, 0.74:1, and 1.29:1, respectively. The morphologies of ZIF-L@ZIF-67[1–4] were similar to the original leaf-shape of the initial ZIF-L template with a slightly rough surface (Fig. 1 and Fig. S3–S5). The PXRD patterns of ZIF-L@ZIF-67[1–4] displayed two characteristic sets of PXRD peaks representing ZIF-L and ZIF-67 (Fig. S2). Elemental mapping images of

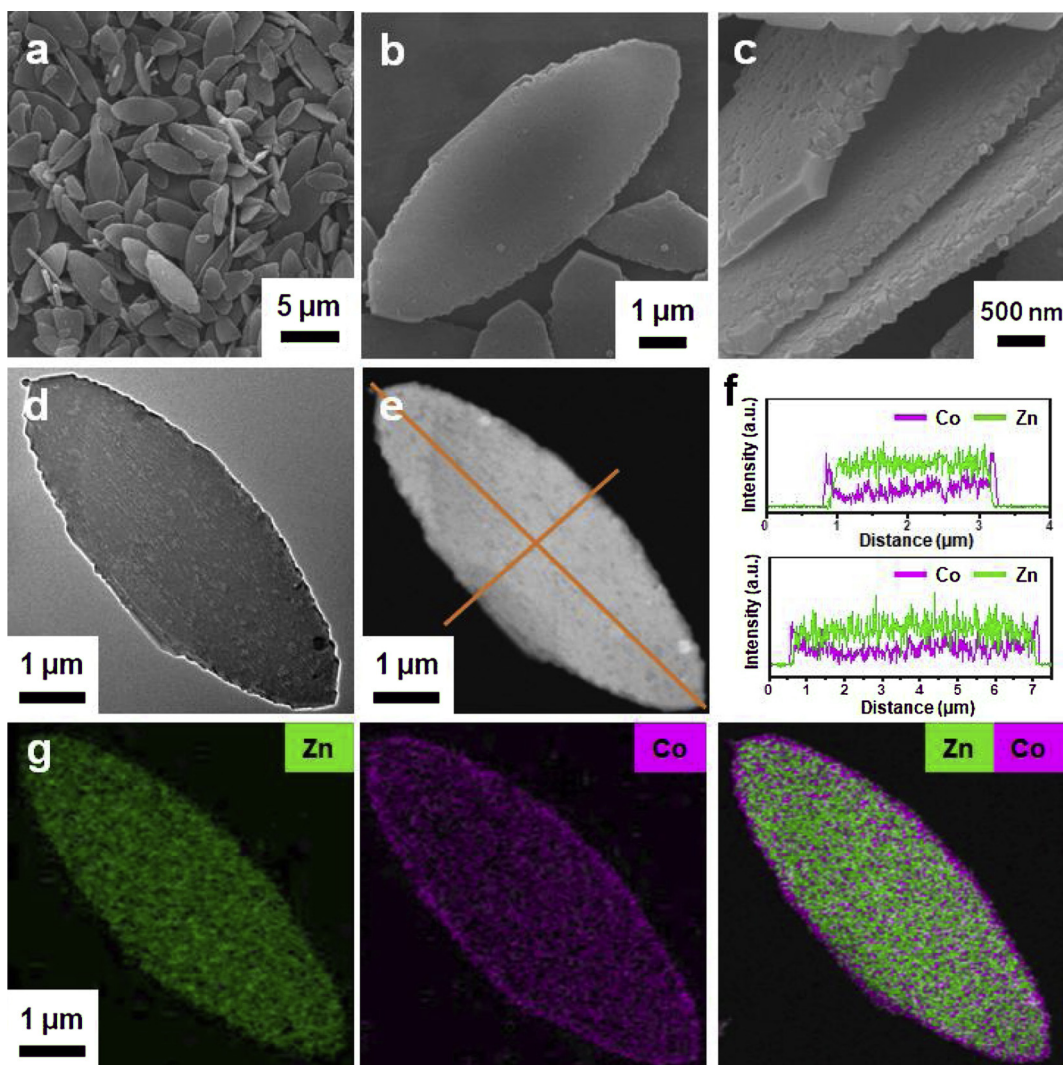


Fig. 1. (a–c) SEM images, (d) TEM, and (e) High-angle annular dark-field scanning transmission electron microscopy (HAADF-STEM) images of leaf-shape ZIF-L@ZIF-67[4]. (f) EDX spectrum profile scanning data measured along the directions marked by the orange lines in (e). (g) Elemental mapping images of ZIF-L@ZIF-67[4] (Zn, green; Co, purple) (For interpretation of the references to colour in this figure legend, the reader is referred to the web version of this article).

ZIF-L@ZIF-67[1–4] revealed that Co atoms as a shell component were distributed within an entire particle; however, Zn atoms as a core component were not detected at the edge of the particle (Fig. 1 and Fig. S3–S5). In addition, EDX spectrum profile scanning data of ZIF-L@ZIF-67[1–4] showed an apparent core–shell structure (ZIF-L@ZIF-67), as demonstrated by the dominant detection of Zn atoms at the center of the particle as a core part and the dominant detection of Co atoms at the edge of the particle as a shell part (Fig. 1 and Fig. S3–S5).

3.2. Cobalt- and nitrogen-codoped porous carbon Co,N-PCL[1–4]

Subsequently, the as-prepared series of ZIF-L@ZIF-67[1–4] was pyrolyzed at 800 °C under N₂. For comparison, pure ZIF-L and ZIF-67 were also pyrolyzed under the same conditions. The color of products after the pyrolysis changed to black from purple or white because of the conversion of ZIF materials to carbon materials. Eventually, Co- and N-codoped porous carbon leaves (Co,N-PCL[1–4]) were obtained from the pyrolysis of ZIF-L@ZIF-67[1–4] while maintaining their original leaf-shape (Fig. 2 and Fig. S10–S12). In particular, scanning electron microscopy (SEM) images showed well-developed carbon nanotubes (CNTs) on the surface of the products (Fig. 2c,d). In addition, high-resolution transmission electron microscopy (HRTEM) images revealed the formation of CNTs, graphitic carbons, and Co nanoparticles. The

lattice fringe images of the product revealed the formation of graphitic carbon with characteristic *d*-spacing of 0.36 nm representing the (002) plane and metallic Co with the *d*-spacing of 0.21 nm representing the (111) plane (Fig. 2g,h). The PXRD pattern (Fig. S13) also revealed the formation of metallic Co as the detected characteristic peaks at ca. 44, 52, and 76° are assigned to the (111), (200), and (220) planes of metallic Co, respectively (PDF no 00-015-0806). The formation of Co nanoparticles during the pyrolysis of Co-containing MOFs and the consequent production of graphitic carbons during the pyrolysis in the presence of Co nanoparticles are well-known phenomena [43–46]. Thus, an increase in the ZIF-67 shell portion (from [1] to [4]) resulted in more Co²⁺ contents, and eventually more Co nanoparticles and CNTs were formed. From the SEM images, we observed that the quantity of CNTs increased with the increase in the ZIF-67 portion (Fig. 2 and Fig. S10–S12). Moreover, increasing the amount of graphitic carbon with the increase in the ZIF-67 shell portion was also confirmed from Raman spectra (Fig. S14). Graphitic carbon including CNT is a very important component to achieve the optimal properties of carbon-based ORR catalysts because it can enhance their conductivity [23–26,37,39]. Additionally, the well-ordered graphitic carbons formed during the pyrolysis and the three-dimensional structural nature of the original ZIF-67 shell make it possible to retain the advantageous original leaf-shape in the case of Co,N-PCLs; however, in the case of C-ZIF-L (the

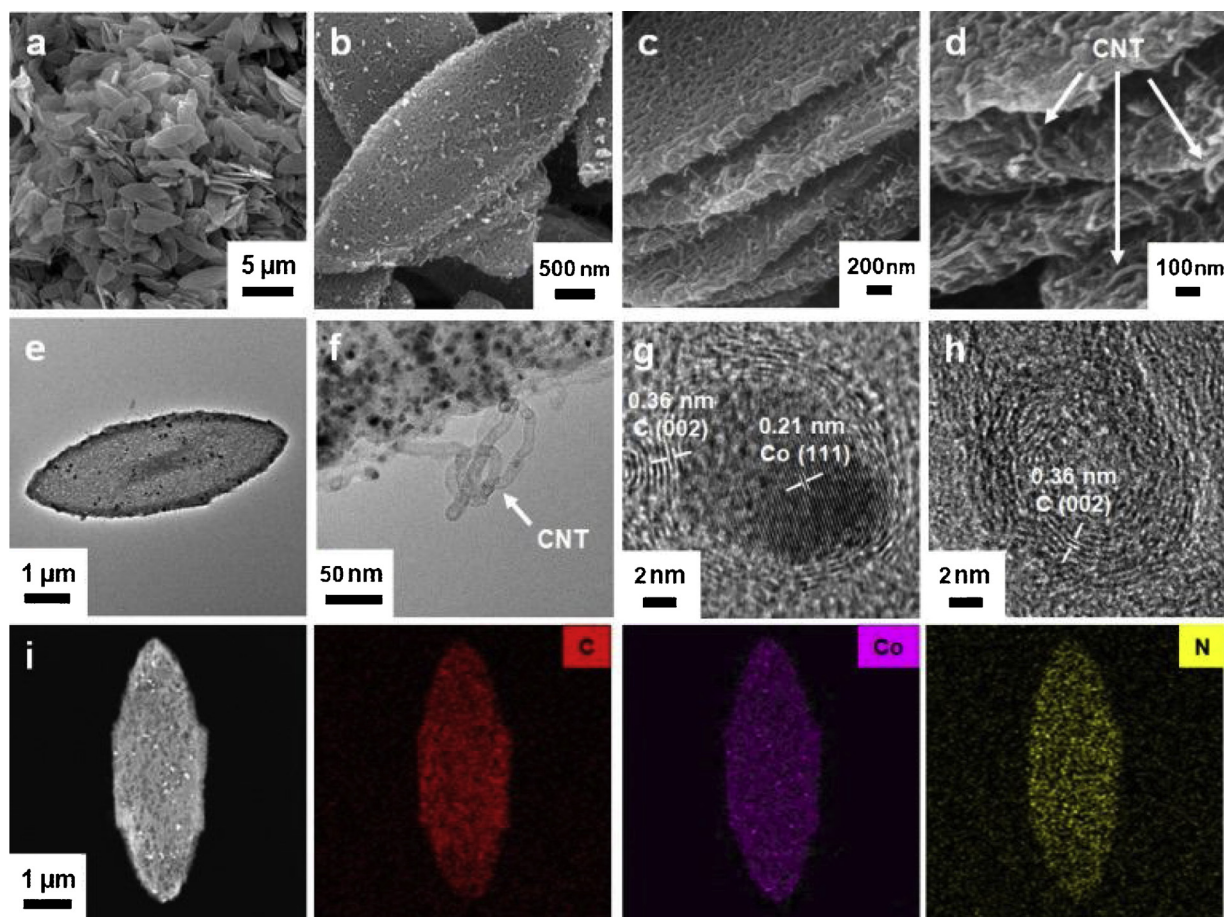


Fig. 2. (a–d) SEM images of Co₃N-PCL[4]. High-magnification SEM image in (d) shows well-developed CNTs. (e,f) TEM images of Co₃N-PCL[4]. (g,h) HRTEM images of Co nanoparticle and graphitic carbons presenting in Co₃N-PCL[4]. (i) HAADF-STEM image and elemental mapping images of Co₃N-PCL[4] (C, red; Co, purple; N, yellow) (For interpretation of the references to colour in this figure legend, the reader is referred to the web version of this article).

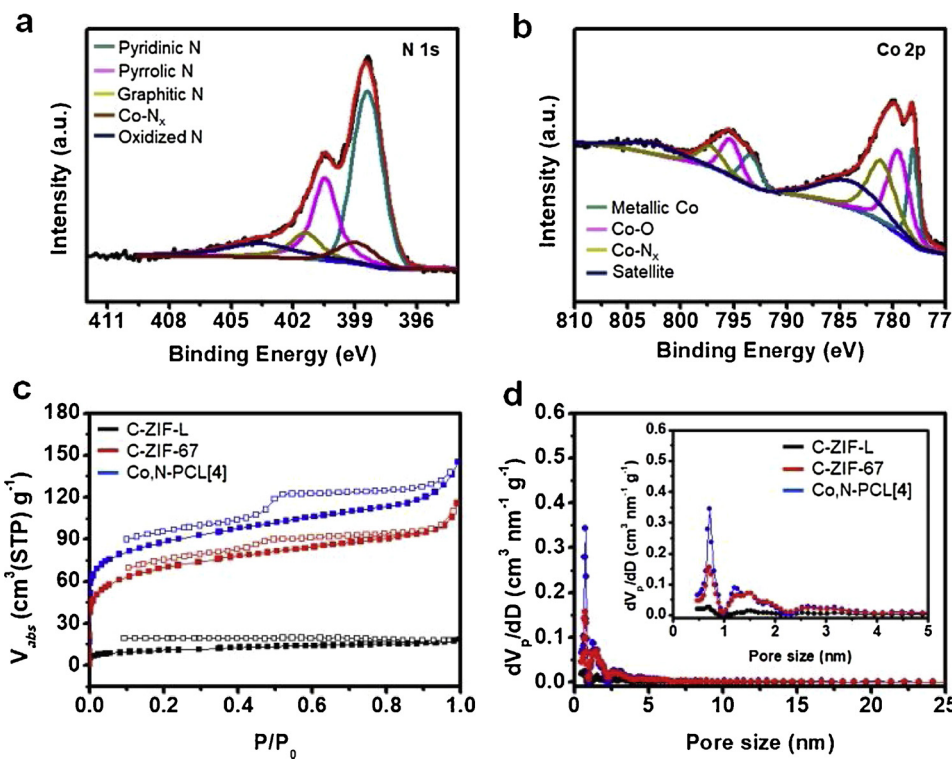


Fig. 3. High-resolution (a) N 1s and (b) Co 2p XPS spectra of Co₃N-PCL[4]. (c) N₂ sorption isotherms of C-ZIF-L (black), C-ZIF-67 (red), and Co₃N-PCL[4] (blue). The filled and open symbols represent the adsorption and desorption branches, respectively. (d) Pore size distributions of C-ZIF-L (black), C-ZIF-67 (red), and Co₃N-PCL[4] (blue) calculated using the non-local density functional theory (NLDFT) (For interpretation of the references to colour in this figure legend, the reader is referred to the web version of this article).

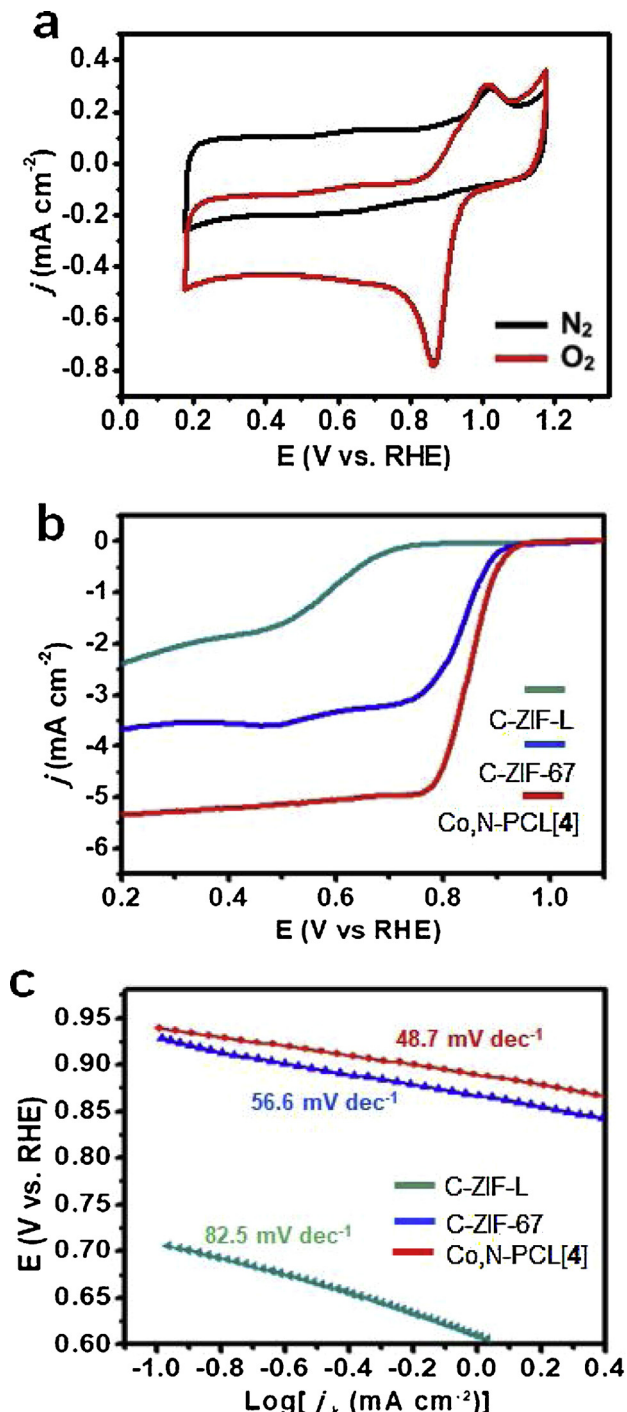


Fig. 4. (a) CV curves of Co,N-PCL[4] in N₂-saturated (black) and O₂-saturated (red) 0.1 M KOH electrolyte. (b) LSV in O₂-saturated 0.1 M KOH electrolyte of C-ZIF-L (green), C-ZIF-67 (blue), and Co,N-PCL[4] (red) at the electrode rotation rate of 1600 rpm. (c) Tafel plots and slopes of C-ZIF-L (green), C-ZIF-67 (blue), and Co,N-PCL[4] (red) (For interpretation of the references to colour in this figure legend, the reader is referred to the web version of this article).

carbon product obtained from the pyrolysis of ZIF-L), the fusion of the resulting carbon product with the adjacent carbon product during the pyrolysis happened and so resulted in the entangled carbon product of a dominant amorphous character with losing its original leaf-shape possibly due to the two-dimensional structural nature of the original ZIF-L (Fig. S8).

The chemical compositions of Co,N-PCL[1–4] were analyzed using EDX, elemental mapping, and X-ray photoelectron spectroscopy (XPS).

It is well known that heteroatom-doping (with atoms such as N, P, and Co) in carbon-based catalysts facilitates the ORR catalytic activity [17–22]. In particular, Co- and N-codoping in carbon-based ORR catalysts induces the structural and electronic alterations, which can provide effective adsorption sites (Co-N moiety) for O₂ and thus increase the ORR activity [20,43,47–49]. First, elemental mapping images of Co,N-PCL[1–4] (Fig. 2 and Fig. S10–S12) showed that the Co and N atoms are simultaneously present through the entire particle. The amount of Co atoms in Co,N-PCL[1–4] increased with the increase in the ZIF-67 portion within ZIF-L@ZIF-67 (from [1] to [4]); however, the amount of N atoms decreased with the increase in the ZIF-67 portion because Co species lead to detach N atoms during the carbonization (Fig. S15) [50,51]. Finally, high-resolution N 1 s XPS spectra revealed the presence of N in the forms of pyridinic N, pyrrolic N, graphitic N, and Co-N_x within Co,N-PCL[1–4] (Fig. 3a and Fig. S17). Among the Co²⁺ ions within the ZIF-67 shell, some were reduced to metallic Co nanoparticles and others existed in the Co-N_x and Co-O forms, as shown in the high-resolution Co 2p XPS spectra of Co,N-PCL[1–4] (Fig. 3b and Fig. S17).

3.3. Electrocatalytic activities of Co,N-PCL[1–4]

The ORR catalytic activity of the as-prepared catalysts was first investigated using cyclic voltammetry (CV) in 0.1 M KOH electrolyte with a three-electrode system. As shown in Fig. 4a, a noticeable redox peak of Co,N-PCL[4] was not observed in N₂-saturated KOH electrolyte. However, the CV curve of Co,N-PCL[4] obtained in O₂-saturated KOH electrolyte displayed a well-defined cathodic peak at approximately 0.863 V versus reversible hydrogen electrode (RHE), indicating its electrocatalytic activity for ORR. To investigate its comprehensive ORR catalytic activity, linear sweep voltammetry (LSV) data of Co,N-PCL[4] and others (C-ZIF-L, C-ZIF-67; the carbon product obtained from the pyrolysis of ZIF-67, and Co,N-PCL[1–3]) were obtained using a rotating disk electrode (RDE) at 1600 rpm (Fig. 4b and Fig. S18). First, more positive half-wave potentials ($E_{1/2}$, 0.822–0.846 V) and higher diffusion-limited current densities (j_i at 0.4 V; 4.64–5.22 mA cm⁻²) were measured from the four Co,N-PCL[1–4] samples compared with those of C-ZIF-L ($E_{1/2} = 0.592$ V and $j_i = 1.86$ mA cm⁻²) and C-ZIF-67 ($E_{1/2} = 0.831$ V and $j_i = 3.56$ mA cm⁻²) (Fig. 4b and Fig. S18). The ORR activity of Co,N-PCL was comparable to that of commercial Pt/C (Fig. S20). Higher diffusion-limited current densities of Co,N-PCL[1–4] indicate efficient mass transport in these samples, which is associated with their thin flat morphological features and high porosity. In addition, Co,N-PCL sample obtained from the 800 °C pyrolysis displayed a best ORR activity among the samples obtained from the pyrolysis at different temperatures (700, 800, or 900 °C, Fig. S21).

Co,N-PCL[1–4] have a leaf shape and this thin flat morphological feature provides several advantages in their ORR activity. For example, the electron transfer and mass transfer involved during the ORR in Co,N-PCL[1–4] can be boosted because numerous active sites are accessible and the catalyst can effectively contact with the reactants related to the ORR [51,52]. In contrast, C-ZIF-L loses a thin leaf morphology of the initial ZIF-L after pyrolysis and has an entangled form, and C-ZIF-67 has a thick dodecahedron morphology, as shown in Fig. S8 and S9. In addition, the N₂ sorption isotherms of Co,N-PCL[4] revealed the presence of micropore and mesopore as shown in the type-I and type-IV isotherm characteristics (Fig. 3c). In particular, Co,N-PCL [4] has a larger surface area (319 m² g⁻¹) and higher porosity (0.22 cm³ g⁻¹) than C-ZIF-L (38 m² g⁻¹ and 0.03 cm³ g⁻¹) and C-ZIF-67 (254 m² g⁻¹ and 0.18 cm³ g⁻¹) (Fig. 3c and Table S1). Higher porosity of carbon-based ORR catalysts can improve the ORR activity by enhancing the mass transport [27–29]. Indeed, Co,N-PCL[4] displayed the highest ORR activity (most positive half-wave potential of 0.846 V and highest diffusion-limited current density of 5.22 mA cm⁻²). In addition, the excellent ORR activity of Co,N-PCL[4] is confirmed by comparing it with other recently developed carbon-based ORR catalysts

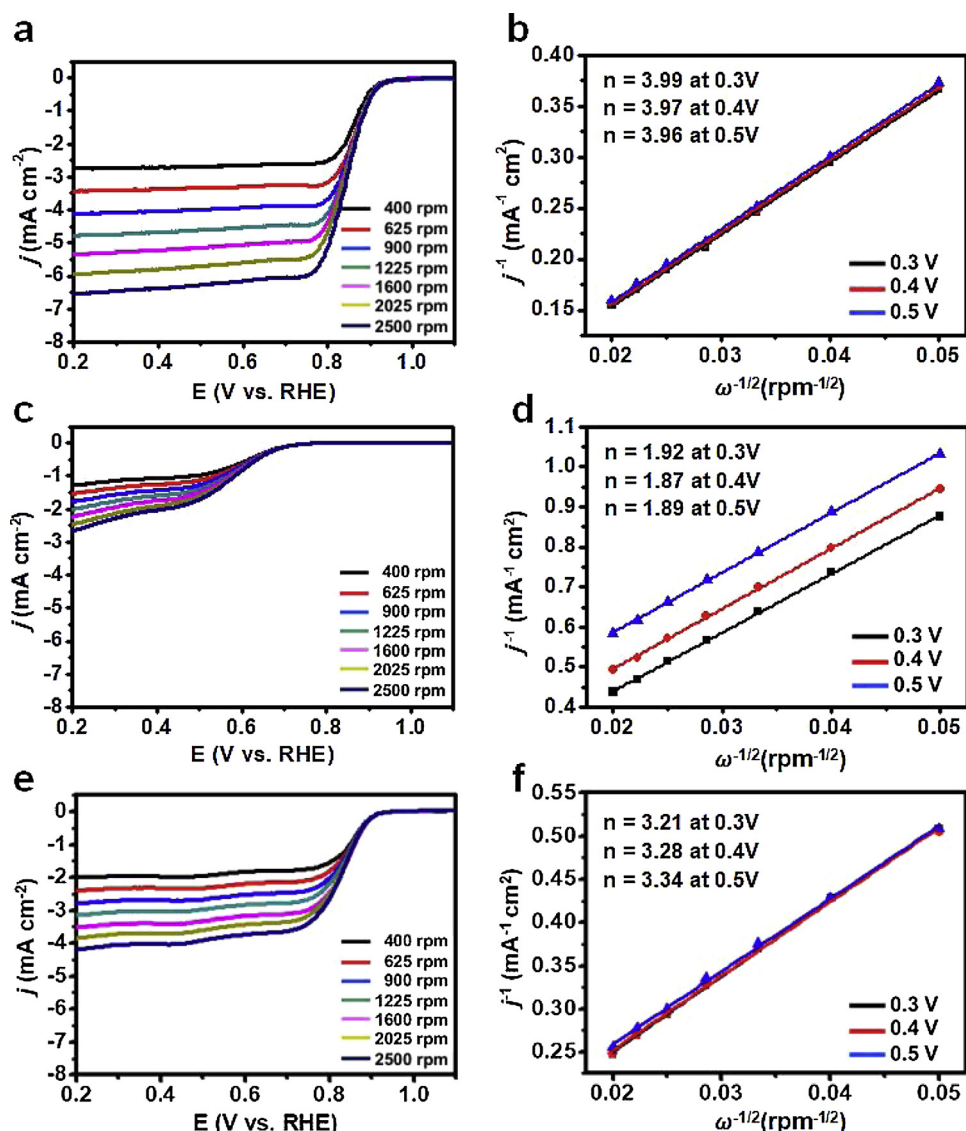
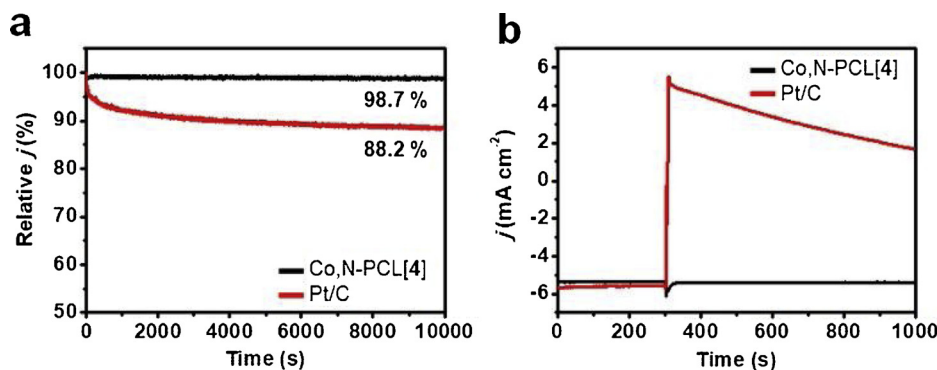


Fig. 5. LSV of (a) Co,N-PCL[4], (c) C-ZIF-L, and (e) C-ZIF-67 measured at various electrode rotation rates (400–2500 rpm). K-L plots of (b) Co,N-PCL[4], (d) C-ZIF-L, and (f) C-ZIF-67 obtained at various potentials (0.3–0.5 V).



(Table S2). The Tafel plots (Fig. 4c) of the products revealed that Co,N-PCL[4] showed a small Tafel slope of 48.7 mV dec^{-1} . This value is smaller than those of C-ZIF-L (82.5 mV dec^{-1}) and C-ZIF-67 (56.6 mV dec^{-1}), indicating that more favorable ORR kinetics occurred in Co,N-PCL[4] [39,44,52].

To obtain detailed information on the ORR mechanism of Co,N-PCL[4], RDE measurements of Co,N-PCL[4] were conducted at various

Fig. 6. (a) Chronoamperometric responses of Co,N-PCL[4] (black) and Pt/C (red) in O_2 -saturated 0.1 M KOH electrolyte at 0.6 V and 1600 rpm. (b) Current-time curves before and after the injection of methanol for Co,N-PCL[4] (black) and Pt/C (red) (For interpretation of the references to colour in this figure legend, the reader is referred to the web version of this article).

rotation rates (400–2500 rpm), which normally display a high current density at high rotation rates [22,51] (Fig. 5a). The electron-transfer number during the catalytic reaction was calculated based on the Koutecky–Levich (K–L) equation. The linearity of the K–L plots of Co,N-PCL[4] indicated first-order reaction kinetics and similar electron-transfer numbers were calculated at different potentials (Fig. 5b). First, the electron-transfer numbers in C-ZIF-L and C-ZIF-67 were calculated

to be 1.89 and 3.28 (Fig. 5d and f), respectively, indicating the formation of a significant amount of HO_2^- . However, the electron-transfer number in $\text{Co}_x\text{N-PCL}[4]$ was much larger than those of its counterparts (C-ZIF-L and C-ZIF-67) and was calculated to be 3.97 (Fig. 5b), indicating the ideal four-electron transfer pathway for efficient ORR activity.

3.4. Electrochemical stability of $\text{Co}_x\text{N-PCL}[4]$

In addition to the catalytic activity, the electrochemical stability of ORR catalysts is of great importance for their practical application. The electrochemical stability of $\text{Co}_x\text{N-PCL}[4]$ was evaluated by measuring its current-time chronoamperometric response in ORR at 0.6 V (Fig. 6a). First of all, commercial Pt/C shows a significant current loss during operation and approximately 88.2% relative current remained after operation for 10,000 s (Fig. 6a). The loss of the initial catalytic activity of Pt/C is known to be attributed to the detachment and/or aggregation of Pt nanoparticles [53,54]. However, $\text{Co}_x\text{N-PCL}[4]$ displayed an excellent electrochemical stability as demonstrated by a persistence of 98.7% relative current after operating for 10,000 s (Fig. 6a). Furthermore, $\text{Co}_x\text{N-PCL}[4]$ displayed no drastic current loss even after a long time operation for 24 h (Fig. S22). In addition to long-term stability, the methanol tolerance of ORR catalysts is another important issue for their methanol fuel cell application. As shown in the current-time curves (Fig. 6b), commercial Pt/C exhibited a critical decay after the injection of methanol into the solution. In contrast, $\text{Co}_x\text{N-PCL}[4]$ displayed a strong tolerance to methanol crossover, as demonstrated by the lack of a significant change after the methanol injection.

4. Conclusions

Co- and N-codoped porous carbon leaves ($\text{Co}_x\text{N-PCls}$) were developed as the effective electrocatalyst for ORR via one-step pyrolysis of the well-designed core–shell type hybrid MOFs (ZIF-L@ZIF-67). The resulting $\text{Co}_x\text{N-PCls}$ retained the advantageous thin leaf-shape of ZIF-L@ZIF-67 because the ZIF-67 shell transformed into highly graphitic carbon materials. In addition, the resulting $\text{Co}_x\text{N-PCls}$ had a high surface area and porosity, which facilitate the mass transfer and electron transfer for ORR. Finally, $\text{Co}_x\text{N-PCls}$ displayed an excellent ORR activity with high positive half-wave potential, high diffusion-limited current density, four-electron transfer mechanism, excellent stability, and good methanol tolerance. These excellent performances could be attributed to their unique structural and compositional features such as thin flat morphology, high surface area/porosity, substantial graphitic carbons including CNTs, and uniform Co- and N-doping. Moreover, $\text{Co}_x\text{N-PCL}[4]$ displays a better stability and a better methanol tolerance than commercial Pt/C. The synthetic strategy demonstrated here should be an excellent and convenient method for the preparation of the efficient carbon-based ORR catalysts with ideal structural and compositional features.

Note

The authors declare no competing financial interest.

Acknowledgements

This work was supported by the National Research Foundation of Korea (NRF) grant funded by the Korea government (MSIP) (no NRF-2017R1A2B3007271).

Appendix A. Supplementary data

Supplementary material related to this article can be found, in the online version, at doi:<https://doi.org/10.1016/j.apcatb.2019.01.083>.

References

- [1] W. Xia, R. Zou, L. An, D. Xia, S. Guo, *Energy Environ. Sci.* 8 (2015) 568–576.
- [2] S. Guo, S. Zhang, S. Sun, *Angew. Chem. Int. Ed.* 52 (2013) 8526–8544.
- [3] J. Liang, R.F. Zhou, X.M. Chen, Y.H. Tang, S.Z. Qiao, *Adv. Mater.* 26 (2014) 6074–6079.
- [4] L. Shang, H. Yu, X. Huang, T. Bian, R. Shi, Y. Zhao, G.I.N. Waterhouse, L.Z. Wu, C.H. Tung, T. Zhang, *Adv. Mater.* 28 (2016) 1668–1674.
- [5] W. Wei, H. Liang, K. Parvez, X. Zhuang, X. Feng, K. Müllen, *Angew. Chem. Int. Ed.* 53 (2014) 1570–1574.
- [6] S. Wang, S.P. Jiang, *Sci. Rev.* 4 (2017) 163–166.
- [7] D. Liu, L. Tao, D. Yan, Y. Zou, S. Wang, *ChemElectroChem* 5 (2018) 1775–1785.
- [8] J. Liang, Y. Zheng, J. Chen, J. Liu, D. Hulicova-Jurcakova, M. Jaroniec, S.Z. Qiao, *Angew. Chem. Int. Ed.* 51 (2012) 3892–3896.
- [9] H.T. Chung, J.H. Won, P. Zelenay, *Nat. Comm.* 4 (2013) 1922–1925.
- [10] Y. Liang, Y. Li, H. Wang, J. Zhou, J. Wang, T. Regier, H. Dai, *Nat. Mater.* 10 (2011) 780–786.
- [11] H. Tang, H. Yin, J. Wang, N. Yang, D. Wang, Z. Tang, *Angew. Chem. Int. Ed.* 52 (2013) 5585–5589.
- [12] H. Yin, H. Tang, D. Wang, Y. Gao, Z. Tang, *ACS Nano* 6 (2012) 8288–8297.
- [13] J. Sun, H. Yin, P. Liu, Y. Wang, X. Yao, Z. Tang, H. Zhao, *Chem. Sci.* 7 (2016) 5640–5646.
- [14] J. Sun, S.E. Lowe, L. Zhang, Y. Wang, K. Pang, Y. Wang, Y. Zhong, P. Liu, K. Zhao, Z. Tang, H. Zhao, *Angew. Chem. Int. Ed.* 57 (2018) 16511–16515.
- [15] D. Yan, L. Guo, C. Xie, Y. Wang, Y. Li, H. Li, S. Wang, *Sci. China Mater.* 61 (2018) 679–685.
- [16] Y. Wang, L. Tao, Z. Xiao, R. Chen, Z. Jiang, S. Wang, *Adv. Funct. Mater.* 28 (2018) 1705356.
- [17] J. Gao, C. He, J. Liu, P. Ren, H. Lu, J. Feng, Z. Zou, Z. Yin, X. Wen, X. Tan, *Catal. Sci. Technol.* 8 (2018) 1142–1150.
- [18] H. Jiang, Y. Zhu, Q. Feng, Y. Su, X. Yang, C. Li, *Chem. Eur. J.* 20 (2014) 3106–3112.
- [19] P. Subramanian, R. Mohan, A. Schechter, *ChemCatChem* 9 (2017) 1969–1978.
- [20] Z. Hu, Z. Zhang, Z. Li, M. Dou, F. Wang, *ACS Appl. Mater. Interfaces* 9 (2017) 16109–16116.
- [21] S. Chao, Z. Bai, Q. Cui, H. Yan, K. Wang, L. Yang, *Carbon* 82 (2015) 77–86.
- [22] Z. Wang, Y. Lu, Y. Yan, T.Y.P. Larissa, X. Zhang, D. Wuu, H. Zhang, Y. Yang, *X. Wang, Nano Energy* 30 (2016) 368–378.
- [23] P. Zhang, F. Sun, Z. Xiang, Z. Shen, J. Yun, D. Cao, *Energy Environ. Sci.* 7 (2014) 442–450.
- [24] L. Zhang, Z. Su, F. Jiang, L. Yang, J. Qian, Y. Zhou, W. Li, M. Hong, *Nanoscale* 6 (2014) 6590–6602.
- [25] S. Gadipelli, T. Zhao, S.A. Shevlin, Z. Guo, *Energy Environ. Sci.* 9 (2016) 1661–1667.
- [26] K. Qiu, Z.X. Guo, *J. Mater. Chem. A Mater. Energy Sustain.* 2 (2014) 3209–3215.
- [27] C. Xuan, B. Hou, W. Xia, Z. Peng, T. Shen, H.L. Xin, G. Zhang, D. Wang, *J. Mater. Chem. A Mater. Energy Sustain.* 6 (2018) 10731–10739.
- [28] Y. Zhang, X. Zhang, X. Ma, W. Guo, C. Wang, T. Asefa, X. He, *Sci. Rep.* 7 (2017) 43366.
- [29] F. Pan, Y. Duan, A. Liang, J. Zhang, Y. Li, *Electrochim. Acta* 238 (2017) 375–383.
- [30] R. Zhao, W. Xia, C. Lin, J. Sun, A. Mahmood, Q. Wang, B. Qiu, H. Tabassum, R. Zou, *Carbon* 114 (2017) 284–290.
- [31] S. Zhao, H. Yin, L. Du, L. He, K. Zhao, L. Chang, G. Yin, H. Zhao, S. Liu, Z. Tang, *ACS Nano* 8 (2014) 12660–12668.
- [32] S. Pandiaraj, H.B. Aiyappa, R. Banerjee, S. Kurungot, *Chem. Commun. (Camb.)* 50 (2014) 3363–3366.
- [33] S. Bhattacharyya, B. Konkena, K. Jayaramulu, W. Schuhmann, T.K. Maji, *J. Mater. Chem. A Mater. Energy Sustain.* 5 (2017) 13573–13580.
- [34] L. Ye, G. Chai, Z. Wen, *Adv. Funct. Mater.* 27 (2017) 1606190.
- [35] R. Banerjee, A. Phan, B. Wang, C. Knobler, H. Furukawa, M. O'Keeffe, O.M. Yaghi, *Science* 319 (2008) 939–943.
- [36] K.S. Park, Z. Ni, A.P. Côté, J.Y. Choi, R. Huang, F.J. Uribe-Romo, H.K. Chae, M. O'Keeffe, O.M. Yaghi, *Proc. Natl. Acad. Sci. U. S. A.* 103 (2006) 10186–10191.
- [37] S. Dou, X. Li, L. Tao, J. Huo, S. Wang, *Chem. Commun. (Camb.)* 52 (2016) 9727–9730.
- [38] R. Li, X. Wang, Y. Dong, X. Pan, X. Liu, Z. Zhao, J. Qiu, *Carbon* 132 (2018) 580–588.
- [39] T. Liu, P. Zhao, X. Hua, W. Luo, S. Chen, G. Cheng, *J. Mater. Chem. A Mater. Energy Sustain.* 4 (2016) 11357–11364.
- [40] R. Chen, J. Yao, Q. Gu, S. Smeets, C. Baerlocher, H. Gu, D. Zhu, W. Morris, O.M. Yaghi, H. Wang, *Chem. Commun. (Camb.)* 49 (2013) 9500–9502.
- [41] W.C. Lee, H.T. Chien, Y. Lo, H.C. Chiu, T.P. Wang, D.Y. Kang, *ACS Appl. Mater. Interfaces* 7 (2015) 18353–18361.
- [42] J. Zhang, Y. Wang, K. Xiao, S. Cheng, T. Zhang, G. Qian, Q. Zhang, Y. Feng, *New J. Chem.* 42 (2018) 6719–6726.
- [43] Y.Z. Chen, C. Wang, Z.Y. Wu, Y. Xiong, Q. Xu, S.H. Yu, H.L. Jiang, *Adv. Mater.* 27 (2015) 5010–5016.
- [44] Y. Hou, Z. Wen, S. Cui, S. Ci, S. Mao, J. Chen, *Adv. Funct. Mater.* 25 (2015) 872–882.
- [45] A. Song, W. Yang, W. Yang, G. Sun, X. Yin, L. Gao, Y. Wang, X. Qin, G. Shao, *ACS Sustain. Chem. Eng.* 5 (2017) 3973–3981.
- [46] S. Wang, Z. Cui, M. Cao, *Chem. Eur. J.* 21 (2015) 2165–2172.
- [47] B. You, N. Jiang, M. Sheng, W.S. Drisdell, J. Yano, Y. Sun, *ACS Catal.* 5 (2015) 7068–7076.
- [48] J. Meng, C. Niu, L. Xu, J. Li, X. Liu, X. Wang, Y. Wu, X. Xu, W. Chen, Q. Li, Z. Zhu, D. Zhao, L. Mai, *J. Am. Chem. Soc.* 139 (2017) 8212–8221.
- [49] B.Y. Xia, Y. Yan, N. Li, H.B. Wu, X.W. (David) Lou, X. Wang, *Nat. Energy* 1 (2016)

15006.

[50] J. Tang, R.R. Salunkhe, J. Liu, N.L. Torad, M. Imura, S. Furukawa, Y. Yamauchi, *J. Am. Chem. Soc.* 137 (2015) 1572–1580.

[51] J. Wei, Y. Hu, Y. Liang, B. Kong, Z. Zheng, J. Zhang, S.P. Jiang, Y. Zhao, H. Wang, *J. Mater. Chem. A Mater. Energy Sustain.* 5 (2017) 10182–10189.

[52] L. Huang, X. Zhang, Y. Han, Q. Wang, Y. Fang, S. Dong, *J. Mater. Chem. A Mater. Energy Sustain.* 5 (2017) 18610–18617.

[53] E.F. Holby, W. Sheng, Y. Shao-Horn, D. Morgan, *Energy Environ. Sci.* 2 (2009) 865–871.

[54] F. Hasché, M. Oezaslan, P. Strasser, *Phys. Chem. Chem. Phys.* 12 (2010) 15251–15258.